

Physics-informed Active Polarimetric 3D Imaging for Specular Surfaces

JIAZHANG WANG^{1,*}, HVELIM YANG¹, TIANYI WANG¹, AND FLORIAN WILLOMITZER^{1,*}

¹*Wyant College of Optical Sciences, University of Arizona, Tuscon, AZ, 85721*
^{*}*jiazhawang@arizona.edu, fwillomitzer@arizona.edu*

Abstract: 3D imaging of specular surfaces remains challenging in real-world scenarios, such as in-line inspection or hand-held scanning, requiring fast and accurate measurement of complex geometries. Optical metrology techniques such as deflectometry achieve high accuracy but typically rely on multi-shot acquisition, making them unsuitable for dynamic environments. Fourier-based single-shot approaches alleviate this constraint, yet their performance deteriorates when measuring surfaces with high spatial frequency structure or large curvature. Alternatively, polarimetric 3D imaging in computer vision operates in a single-shot fashion and exhibits robustness to geometric complexity. However, its accuracy is fundamentally limited by the orthographic imaging assumption.

In this paper, we propose a physics-informed deep learning framework for single-shot 3D imaging of complex specular surfaces. Polarization cues provide orientation priors that assist in interpreting geometric information encoded by structured illumination. These complementary cues are processed through a dual-encoder architecture with mutual feature modulation, allowing the network to resolve their nonlinear coupling and directly infer surface normals. The proposed method achieves accurate and robust normal estimation in single-shot with fast inference, enabling practical 3D imaging of complex specular surfaces.

1. Introduction

Accurate and robust 3D imaging of specular surfaces plays a critical role in a wide range of applications, including industrial inspection [1, 2], cultural heritage preservation [3], and robotic perception [4]. Nevertheless, achieving fast and reliable reconstruction in real-world scenarios remains challenging. First, the motion-robust measurements are required in applications such as in-line inspection on moving conveyor belts or hand-held 3D scanning systems [3]. In addition, the target objects often exhibit complex geometries, especially large curvature and high spatial frequency. Both of them pose significant challenges to existing methods.

In optical metrology, deflectometry [5–7] is a representative technique that provides high-accuracy measurement of specular surfaces. Its performance depends on the precise camera-screen correspondence, which is typically established through multi-shot acquisition of sequential structured light patterns, such as phase-shifting methods [8]. This sequential strategy, however, is incompatible with high-speed or dynamic measurement scenarios. Single-shot deflectometry approaches have been demonstrated [6, 9], for example, by displaying a cross-sinusoidal pattern and retrieving the correspondence via Fourier-based analysis. However, the complex surface geometries targeted in this work strongly deviate from the low frequency object (e.g., “spherical lens shape”) that is typically measured with deflectometry. The high spatial frequency or large curvature of these surfaces induce large frequency variation of the reflected pattern. As a result, Fourier-based methods suffer from bandwidth limitations, leading to performance degradation. Although windowed Fourier transform [10] or wavelet transform-based methods [6, 9] has been explored to alleviate this issue, such approaches often lack robustness in the presence of noise and introduce substantial computational overhead which prevents potential real-time evaluation. Even if the phase can be successfully retrieved, phase unwrapping is required to

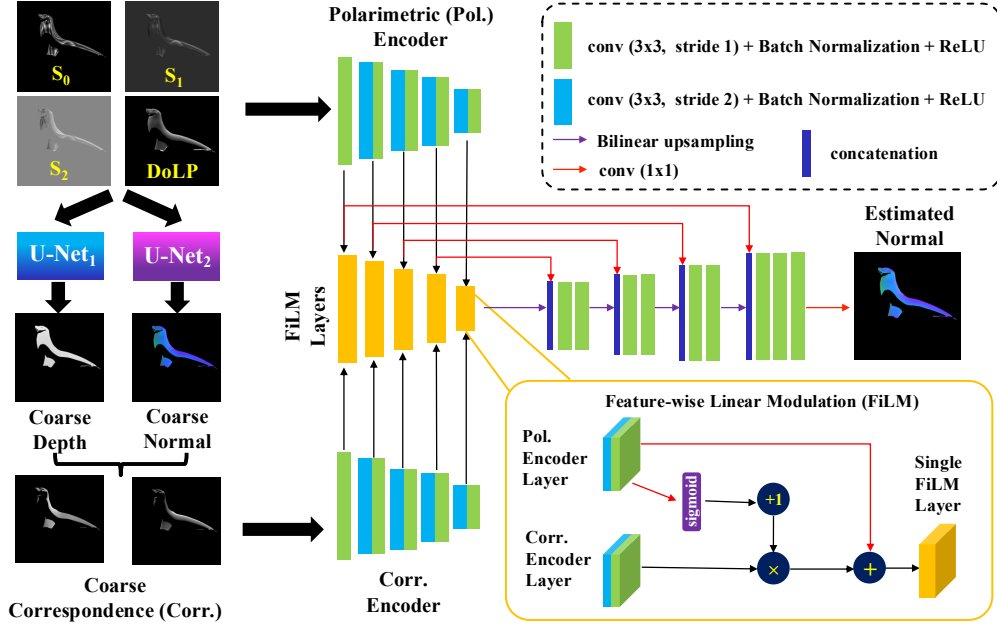


Fig. 1. **Overview of the proposed physics-informed learning framework.** Polarimetric inputs, including Stokes parameters and DoLP, are first processed by U-Nets to obtain coarse depth and normal estimates. Then the coarse correspondence map is analytically calculated. These physics priors are processed separately through two encoder branches to extract modality-specific features. Feature-wise Linear Modulation layers are employed to adaptively fuse polarimetric cues and geometric correspondence features, enabling robust normal estimation.

recover continuous camera-screen correspondence. This process typically relies on additional patterns, compromising the single-shot nature of the system, or requires strong surface priors, further limiting the practicality and robustness of standard deflectometry. Moreover, the inherent depth–normal ambiguity [6, 11] in single-camera deflectometry further restricts its applicability to full-field 3D measurements. Although stereo deflectometry [5, 6] resolves this ambiguity, it significantly reduces the effective measurement region.

As an alternative, computer vision techniques offer greater flexibility and robustness in practical scenarios and are generally less sensitive to geometric complexity. Among them, polarimetric 3D imaging [12–14] enables single-shot measurement of specular surfaces in a passive manner by exploiting polarization cues. However, besides the long-standing normal ambiguity issue [13, 14], its measurement accuracy is fundamentally constrained by the oversimplified orthographic imaging assumption, which treats reflected rays as perpendicular to the image plane. This simplification conflicts with the physics of perspective imaging present in most systems. As a result, significant surface normal errors can arise, typically exceeding 5° and in some cases reaching several tens of degrees. These limitations hinder the adoption of polarimetric imaging in applications demanding high accuracy, such as robotic manufacturing and medical imaging.

Our previous work [11] introduced a multi-modal 3D imaging framework that integrates polarimetric and geometric cues, enabling surface reconstruction without depth–normal ambiguity or reliance on the orthographic imaging assumption. Despite these advantages, the method remains limited in practical applications. First, it still encounters challenges in establishing reliable camera-screen correspondence under single-shot acquisition when measuring complex geometries with high spatial frequencies or large curvature. Second, as a purely analytical

formulation that tightly couples polarimetric and geometric measurements, the reconstruction follows a deterministic computation pipeline. Noise or estimation errors in either modality directly propagate through this pipeline and may be amplified, leading to degraded performance.

In this contribution, we address these issues by leveraging a physics-informed deep neural network. In the first stage, instead of explicitly computing the camera-screen correspondence, we input the polarization priors to the network to estimate the correspondence map. In the second stage, physics priors (polarization and geometric cues) are processed by two separate encoder branches to extract complementary features. These features are subsequently fused in a shared decoder, where cross-modal feature modulation is introduced to mitigate error propagation from individual modalities. The proposed method exhibits strong robustness to unseen objects while maintaining high accuracy. The mean angular error of the estimated normals is 0.79° , significantly outperforming conventional polarimetric 3D imaging approaches. Its single-shot capability and fast inference improve the practicality and efficiency compared to conventional optical metrology systems.

2. Method

The proposed method jointly exploits polarimetric and geometric information to estimate the surface normals of specular objects. Polarimetric cues encode surface orientation by providing the reflection angle between the surface normal and the viewing direction. Geometric information, obtained from the screen’s structured illumination, establishes the correspondence between the light source emission point (screen pixel) and the camera pixel observing the reflected ray. In ideal conditions, these complementary modalities uniquely determine the surface shape. A detailed description of how the multimodal information is acquired is presented in our previous work [11], which used an analytical formulation for evaluation.

In this work, we adopt the same system configuration consisting of an unpolarized display screen and a polarization camera capable of capturing four images at different polarization angles in a single-shot. The first stage of the proposed method aims to mitigate the difficulty of establishing camera–screen correspondence from a single-shot pattern (e.g., a cross-sinusoidal pattern). Instead of explicitly analyzing the deformed fringe pattern in the frequency domain, we leverage polarimetric cues. Given four polarization images $I_0, I_{45}, I_{90}, I_{135}$ captured at polarizer angles $0^\circ, 45^\circ, 90^\circ$, and 135° , we compute the Stokes parameters and the degree of linear polarization (DoLP) as follows:

$$S_0 = \frac{1}{2}(I_0 + I_{45} + I_{90} + I_{135}), \quad S_1 = I_0 - I_{90}, \quad (1)$$

$$S_2 = I_{45} - I_{135}, \quad \text{DoLP} = \frac{\sqrt{S_1^2 + S_2^2}}{S_0}. \quad (2)$$

Beyond encoding surface orientation, the Stokes vectors also preserve the pattern deformation. This deformation, induced by specular reflection, implicitly contains geometric information about surface shape. Therefore, the polarimetric representation not only provides surface orientation priors but also carries active-illumination-induced geometric cues.

These polarimetric physics priors are fed into two separate U-Net models to predict coarse surface depth and normals (see Fig. 1). According to the law of specular reflection, and given the predicted depth and normal together with calibrated camera intrinsics, the viewing direction and corresponding incident ray can be determined. With the calibrated screen pose, the intersection between the incident ray and the screen plane is computed to recover the corresponding screen emission pixel.

The second stage aims to reduce error amplification caused by noise and uncertainty, which may propagate through the analytical reconstruction pipeline. To more effectively exploit the

complementary physics information (polarimetric and geometric cues) while mitigating error propagation, we feed the data into two independent encoder branches (polarimetric encoder and correspondence encoder) to extract modality-specific features (see Fig.1).

The geometric cues, represented by the coarse correspondence map, may be unreliable in regions with high spatial frequency or large curvature. To address this issue, we introduce a feature-wise linear modulation (FiLM) layer [15], where polarization features are used to modulate the geometric features. This mechanism enables the network to adaptively weight geometric information according to the local polarization state, thereby suppressing unreliable geometric estimates. The modulated geometric features are then fused with polarization features in a shared decoder to predict the final surface normal map. The network is trained using a masked mean angular error loss and optimized with Adam optimizer, with an initial learning rate of 1×10^{-4} scheduled by cosine annealing.

Data quality plays a critical role in the performance of learning-based 3D imaging methods. However, acquiring reliable ground-truth data for challenging real world specular surfaces remains difficult for several reasons. First, most off-the-shelf specular objects do not provide ground-truth surface normals. Second, ultra-high-precision measurement systems, such as stereo deflectometry or interferometry, are difficult to deploy in large-scale data collection due to their complexity and limited throughput. Third, many learning-based polarimetric methods rely on commercial 3D scanners to obtain surface depth and subsequently compute normals via numerical differentiation. However, most commercial 3D scanners (e.g., stereo vision or time-of-flight systems) are primarily designed for diffuse reflection-dominated surfaces and typically perform poorly on specular objects. In addition, their accuracy is often insufficient for high-precision tasks and may not exceed the performance level targeted by our method. Even when depth can be recovered, numerically differentiating depth maps often introduces noise, making the resulting normals unreliable as ground truth.

To address these challenges, we generate training data using a physics-based rendering engine, Mitsuba [16]. We construct a digital twin of our experimental setup (see Fig. 2(a)) in a virtual environment, replicating the camera intrinsics, screen pose, and illumination patterns. This enables the synthesis of physically consistent polarization images along with accurate ground-truth surface normals. The dataset consists of 38 distinct 3D objects collected online. Each object is rendered under varying poses and viewpoints, resulting in 605 unique samples. All images are generated at a resolution of 1024×1024 for four polarization angles consistent with our real polarization camera setup. To better approximate real measurements, random noise is added to each rendered image, with the signal-to-noise ratio controlled between $40dB$ and $50dB$.

3. Experiments and Discussion

Fig. 2(a) shows our real setup consisting of a polarization camera (model: FLIR BFS-US-51S5PC-C) and an unpolarized display (model: BOOX Tablet Tab). The system is pre-calibrated for the purpose of building the digital twin in the virtual environment to generate training data. All experiments are conducted on a workstation equipped with an Intel Core i9-14900F CPU, 32GB of memory, and an NVIDIA GeForce RTX 5070 Ti GPU.

To evaluate the performance of the proposed network, we test it on a set of unseen objects that is not included in the training dataset. Fig. 3 shows an example. After the first stage, the estimated coarse normal map achieves a mean angular error of 2.0° compared to the ground truth. After the second stage, refined by both polarimetric cues and geometric cues, the final estimated surface normal map is shown in Fig. 3(b) and compared against the ground-truth normal map. The angular error map is visualized in Fig. 3(d). Our method achieves a **mean angular error of 0.79°** . Furthermore, as summarized in Table 1, **73.23%** of the measurement area exhibits an angular error below 1° , and **93.64%** are below 2° , indicating high accuracy and robustness.

For comparison, we also evaluate the conventional polarimetric 3D imaging method [13] on

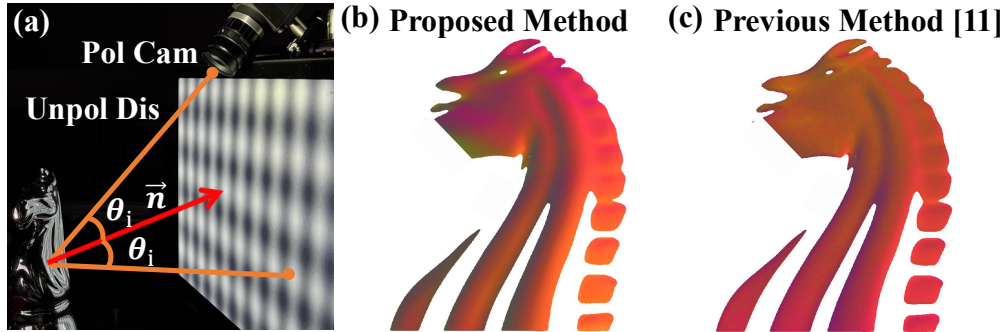


Fig. 2. **Real experimental prototype and qualitative comparison.** (a) The prototype consists of a polarization camera and an unpolarized display. (b) Surface normal estimated by the proposed method with single-shot capture. (c) Surface normal estimated using the previous physics-based method [11] with multi-shot sequential captures. The proposed method produces a more consistent normal field, especially in facial region of the horse.

the same object. To avoid additional errors caused by normal ambiguity, we disambiguate both the zenith and azimuth angles using the ground-truth geometry. As illustrated in Fig. 3(c), the angular error of the conventional polarimetric 3D imaging method increases from the image center toward the periphery. This behavior is a direct consequence of its assumption of the orthographic imaging model, which becomes increasingly inaccurate under a perspective camera model. Quantitatively, it yields a **mean angular error of 4.20°** . Only **6.82%** of the valid pixels achieve an error below 1° , and **20.32%** fall below 2° , as reported in Table 1.

Overall, the comparison clearly shows that the proposed method significantly outperforms the conventional polarimetric 3D imaging method, particularly for regions away from the image center.

To further validate the performance of the proposed network on real-world data, we input the images captured with our real prototype. We first conduct a qualitative evaluation on a complex-shaped object (see Fig. 2(b)). For comparison, Fig. 2(c) presents the result obtained from our previous analytical solution [11], which had to rely on multi-shot captures for this degree of object complexity. As observed, the previous method exhibits noticeable noise and local inconsistencies, particularly in the facial region of the horse, where the surface appears overly flat and lacks structural details. In contrast, our method produces a significantly more consistent normal field while preserving fine geometric structures. In addition, the inference time of the proposed method is $8ms$, which is several orders of magnitude faster than the purely physics-based method.

For quantitative evaluation, we measure a precisely manufactured bearing ball, whose ground-truth normal can be analytically derived by assuming the object is a perfect sphere. The reconstructed normals yield a mean angular error of 1.48° . Although this error is higher than that observed in simulation, the discrepancy can be attributed to real-world factors that are not fully simulated in the current rendering model. In practical polarization cameras, polarization is realized through a pixel-level micro-polarizer array. Due to the angular misalignment of polarization axes, and inter-pixel optical leakage, the measured intensity at each polarization angle inevitably contains cross-channel contamination. Furthermore, demosaicing and interpolation processes introduce additional estimation uncertainty in the Stokes parameters. Combined with material inhomogeneity and non-ideal reflectance behavior of real surfaces, these factors affect the stability of the computed Stokes vectors and DoLP. These physical imperfections are not fully modeled in our virtual dataset, indicating opportunities for more accurate data generation in

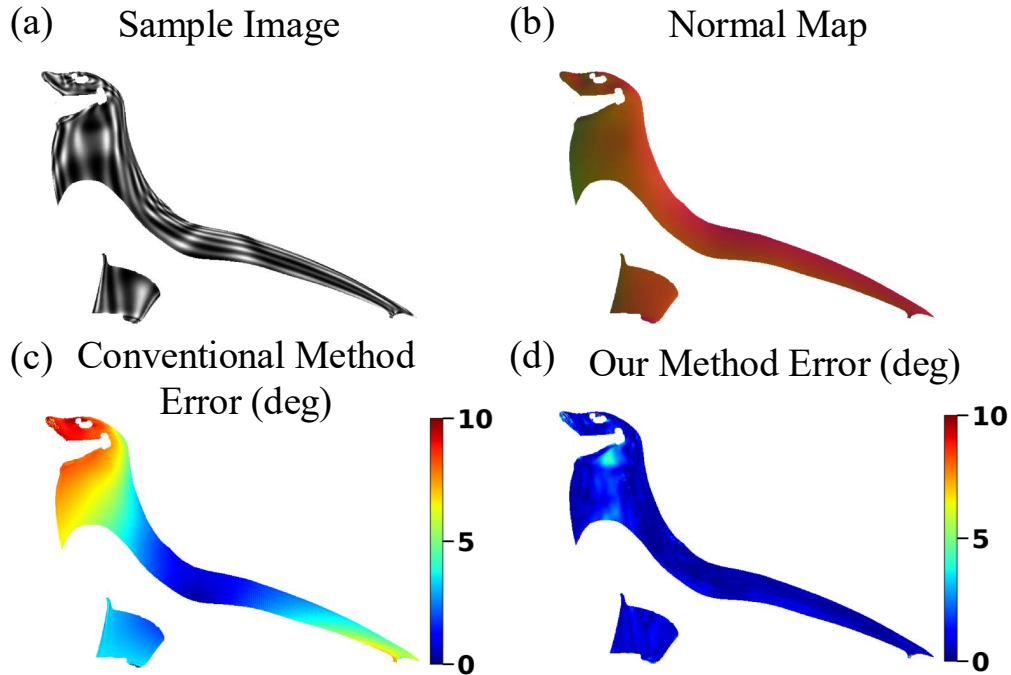


Fig. 3. **Quantitative evaluation.** (a) Sample input image under cross-sinusoidal illumination. (b) Estimated surface normal map using the proposed method. (c) Angular error map of the conventional polarimetric 3D imaging method [13]. (d) Angular error map of the proposed method.

future work.

Table 1. Surface normal estimation error statistics on the unseen object.

Method	$< 1^\circ$ (%)	$< 2^\circ$ (%)	$< 3^\circ$ (%)
Ours	73.23	93.64	97.45
Conventional [13]	6.82	20.32	37.51

Conclusion and discussion: The proposed method demonstrates strong generalization and robustness under single-shot acquisition while keeping the high accuracy. It achieves geometrically consistent full-field reconstruction even for surfaces with high spatial frequency structures and large curvature, where conventional single-shot methods fail to provide reliable measurement. Compared with previous analytical approaches, our method offers improved stability and faster inference in practical scenarios.

Despite our encouraging first results, several directions remain for further improvement. Although the network was trained on synthetic data simulated from the digital twin, extending the training data to incorporate a wider range of real sensor characteristics would further enhance generalization. Future work may explore improved sensor-level modeling and hybrid training strategies that combine synthetic and real measurements. In addition, the current framework is specifically designed for specular surfaces. Polarimetric 3D imaging is intrinsically influenced by material properties, and different materials may exhibit distinct polarization responses governed

by different reflection models. Extending the proposed approach to handle a broader class of materials, including mixed or spatially varying reflectance, remains an important direction for future research. We hope the proposed method will contribute to more practical and deployment-efficient 3D imaging solutions for complex specular surfaces in dynamic environments.

Disclosures. The authors declare no conflicts of interest.

Data availability. Data underlying the results presented in this Letter are available upon reasonable request.

References

1. J. Burke, A. Pak, S. Höfer, M. Ziebarth, M. Roschani, and J. Beyerer, “Deflectometry for specular surfaces: an overview,” *Adv. Opt. Technol.* **12** (2023).
2. J. Dai, W. Zeng, W. Zhong, X. J. Jiang, and W. Lu, “Nonlinear error compensation algorithm for signal resolution of chromatic confocal measurements,” *Measurement* **226**, 114091 (2024).
3. F. Willomitzer, C.-K. Yeh, V. Gupta, W. Spies, F. Schiffers, A. Katsaggelos, M. Walton, and O. Cossairt, “Hand-guided qualitative deflectometry with a mobile device,” *Opt. express* **28** (2020).
4. Y. Li, F. Gao, Y. Xu, W. Wu, Y. Yu, N. Gao, Z. Meng, Z. Zhang, X. Zhang, and X. Jiang, “Robotic near optical coaxial phase measuring stitching deflectometry for form measurement of specular surfaces,” *Opt. Express* **33**, 36146–36162 (2025).
5. M. C. Knauer, J. Kaminski, and G. Häusler, “Phase measuring deflectometry: a new approach to measure specular free-form surfaces,” (SPIE, 2004).
6. J. Wang, T. Wang, B. Xu, O. Cossairt, and F. Willomitzer, “Accurate eye tracking from dense 3d surface reconstructions using single-shot deflectometry,” *Nat. Commun.* **16**, 2902 (2025).
7. A. Dashpute, J. Wang, J. Taylor, O. Cossairt, A. Veeraraghavan, and F. Willomitzer, “Event-based motion-robust accurate shape estimation for mixed reflectance scenes,” *arXiv preprint 2311.09652* (2023).
8. C. Zuo, S. Feng, L. Huang, T. Tao, W. Yin, and Q. Chen, “Phase shifting algorithms for fringe projection profilometry: A review,” *Opt. lasers engineering* **109**, 23–59 (2018).
9. H. Liang, T. Sauer, and C. Faber, “Using wavelet transform to evaluate single-shot phase measuring deflectometry data,” in *Applications of Digital Image Processing XLIII*, vol. 11510 (SPIE, 2020), pp. 404–410.
10. Q. Kemao, “Windowed fourier transform for fringe pattern analysis,” *Appl. Opt.* **43** (2004).
11. J. Wang, O. Cossairt, and F. Willomitzer, “3d imaging of complex specular surfaces by fusing polarimetric and deflectometric information,” *Optica* **12**, 446–450 (2025).
12. S. Rahmann and N. Canterakis, “Reconstruction of specular surfaces using polarization imaging,” in *CVPR*, vol. 1 (IEEE, 2001).
13. G. A. Atkinson and E. R. Hancock, “Recovery of surface orientation from diffuse polarization,” *IEEE transactions on image processing* **15** (2006).
14. A. Kadambi, V. Taamazyan, B. Shi, and R. Raskar, “Polarized 3d: High-quality depth sensing with polarization cues,” in *ICCV*, (2015).
15. E. Perez, F. Strub, H. De Vries, V. Dumoulin, and A. Courville, “Film: Visual reasoning with a general conditioning layer,” in *AAAI*, vol. 32 (2018).
16. W. Jakob, S. Speierer, N. Roussel, M. Nimier-David, D. Vicini, T. Zeltner, B. Nicolet, M. Crespo, V. Leroy, and Z. Zhang, “Mitsuba 3 renderer,” (2022). <https://mitsuba-renderer.org>.